An Airjet Actuator System for Identification of the Human Arm Joint Mechanical Properties

Yangming Xu, *Student Member, IEEE*, Ian W. Hunter, *Member, IEEE*, John M. Hollerbach, *Member, IEEE*, and David J. Bennett, *Student Member, IEEE*

Abstract—A system is described for determining the mechanical properties of the human arm during unconstrained posture and movement. An airjet perturbation device is attached to the wrist with a special cuff, and provides high-frequency stochastic perturbations in potentially three orthogonal directions. The airjet operates as a fluidic flip-flop utilizing the Coanda effect, and generates binary force sequences with a steady-state thrust of 4 N, a flat frequency response to 75 Hz, usable thrust to 150 Hz, and a rise time of 1 ms, when the static pressure at the nozzle inlet is 5.5×10^5 Pa (80 psi). These operating characteristics are adequate to identify the arm's mechanical properties efficiently and robustly.

I. INTRODUCTION

TO understand how the human motor control system controls free arm movements, an important piece of information is how the arm behaves when it is mechanically perturbed under different movement conditions, such as changes in speed, hand-held loads, and target locations. Hypotheses about motor control can be devised and tested, based on detailed predictions of how the mechanical properties of the arm change during the motion and between movement tasks. Moreover, for clinical diagnosis and monitoring, normal mechanical behavior of the human could be quantitatively compared to abnormal mechanical behavior, experimentally measured in the same way, of individuals with motor deficits. This knowledge could also be of use in prosthetics, by setting goals for life-like prosthetic arm behavior, and in robotics, as an example of a natural solution to the motion control problem.

Knowledge of the joint mechanical properties of the human arm during posture and movement has until recently been limited to single-joint movements because instrumentation has not been available to apply appropriate spatial perturbations to the arm and to measure accurately the resulting displacements. This paper reports on new instrumentation whose ultimate purpose is to perturb arbitrary and natural multijoint human arm movements, to measure accurately the force of perturbation and the resulting displacements, and to allow the application of nonlinear stochastic system identification techniques to characterize the joint mechanical properties.

Previous arm studies have primarily used electric motors for perturbations. Advantages of electric motors are that power amplifiers and servo systems are readily available commercially, and that accurate position transducers are easily incorporated to measure rotor motion. Disadvantages include bulkiness and a low ratio of force or torque to mass. Rotary motors typically can only apply low-frequency perturbations because of the large rotor inertia and limitations in the power amplifiers. While linear motors can generate high perturbation frequencies, their limited range of motion is most appropriate for postural rather than motion studies. Consequently, electric motors have been primarily applied to single-joint perturbation. In one configuration, the upper arm and forearm are strapped or cast into a single degree-of-freedom mechanical linkage, and the motor axis directly exerts torque on the coincident linkage and elbow joints [9], [23], [35]. In another configuration, the elbow point is fixed and a force is exerted directly on the wrist by an attached rod or cable running to the motor [22], [36], [16]. Planar two-dimensional perturbations have been applied to the hand or wrist with two-link, parallel drive mechanisms driven by electric motors [29].

Perturbations have also been applied by hydraulic actuators, which offer advantages of much higher force or torque over electric motors for a given size. Depending on the servo-valve design, they may also provide a higher frequency output. They have been applied to the elbow [4] and to the ankle [18].

Neither hydraulic actuators nor electric motors lend themselves readily towards a three-dimensional perturbation device. Although transmission elements such as rods or cables are conceivable, the dynamics of such elements are likely to confound the arm dynamics and to limit the perturbation bandwidth.

Recently, pneumatic thrusters have been devised as perturbation devices [8], [28] where compressed air is the power source and hydraulic spool valves control the air flow. Since airjet nozzles can be mounted on a cuff at-

tached to the wrist, they offer the possibility of multidimensional perturbations without significant constraints on arm movement. The tubing running to the cuff is light and flexible and does not impede movement, and the expelled air is of course not an environmental problem. These airjet systems therefore represent a major advance in instrumentation because the experimentally imposed arm movement constraint is eliminated. A disadvantage of the spool valve design in these airjets is spool mass and the resulting limitation on the system frequency bandwidth to about 20 Hz [8].

For any perturbation device designed to infer the human elbow's joint mechanical properties, a high frequency bandwidth is essential. There is reason to believe that these properties are nonlinear and time-varying (in analogy to the ankle joint [15]), and a high-frequency stochastic input is the best input to identify them [10], [24], [25]. Even if a linear model is assumed, a high frequency is required to identify inertia reliably.

In this paper, we present a new airjet design using as the primary control a fluidic switching device, based on the Coanda effect. Our design greatly reduces the mass of mechanical moving parts and enhances the frequency bandwidth dramatically. This airjet is intrinsically a bistable device that can generate arbitrary binary force sequences, such as pseudorandom binary sequences (PRBS), colored white noise, and Walsh functions. In our studies to date, we have used PRBS, which are the most efficient implementation of a Gaussian white noise signal [14]. An additional part of the system is the Optotrak™ (Northern Digital Inc., Waterloo, Ont.), a three-dimensional motion tracking system whose resolution is 0.05 mm. The recent emergence of such high-accuracy measurement systems is essential for unrestrained arm movement studies in general and for our perturbation studies in particular.

II. SPECIFICATIONS

We require that the airjet system 1) not change the properties of the system under study significantly, 2) perturb the system with enough power for high signal-to-noise ratio measurements, and 3) excite the system with adequate bandwidth for robust system identification. These specifications require some prior knowledge of the system and of the displacement-measuring apparatus's capability. Here we will consider the human elbow joint as the system under study, even though the airjet system design is not restricted to the forearm only.

Displacements are measured by the Optotrak, which uses three cameras to triangulate active markers [infrared light-emitting diodes (IRED's)] attached to the moving segment. Each camera contains a 2048 element linear CCD array and a cylindrical lens, which columnates the IRED beams. Due to a Gaussian spread of the light envelope, processes of thresholding and subpixel localization result in a dynamic range of $10^5 : 1$. The cameras are embedded in a solid aluminum block and are automatically calibrated by accompanying software. The resolu-

tion is 0.05 mm in a 0.25 m³ viewing volume, and the highest sampling rate is 250 Hz for one IRED. If the perturbated motion has an rms value of 0.2 mm, the signal-to-noise ratio may be loosely calculated as $SN = 0.2/0.05 = 4$. Therefore, a minimum 0.2 mm perturbation is required at the highest frequency. This requirement will be used to estimate the amplitude of the force.

The most ubiquitous perturbation model in human motor control research is the second-order linear model. For single-joint movement, such as at the elbow,

$$I\ddot{\theta}_p + B\dot{\theta}_p + K\theta_p = \tau_p \qquad (1)$$

where τ_p is the perturbation force, θ_p, $\dot{\theta}_p$, $\ddot{\theta}_p$ are the joint position, velocity, and acceleration, and the mechanical impedance parameters I, B, K are the limb inertia, the joint viscosity, and the joint stiffness. The mechanical impedance parameters B and K are commonly regarded as changing quantities controlled by the central nervous system (CNS); (1) represents a quasilinear model applicable only about a specific operating point, e.g., some mean muscle activation level. I is usually reasonably constant during single-joint movement. This linear perturbation model will be used to specify the perturbation force τ_p in terms of its type, frequency bandwidth, and amplitude.

The required frequency range can be determined from (1) with *a priori* knowledge on the possible values of the parameters I, B, K. The transfer function is obtained via the Laplace transform:

$$\frac{\theta_p}{\tau_p} = \frac{1}{Is^2 + Bs + K} = \frac{1}{K} \frac{\omega_n^2}{s^2 + 2\xi\omega_n s + \omega_n^2} \qquad (2)$$

where $\omega_n = \sqrt{K/I}$ is the natural frequency and $\xi = B/2\sqrt{IK}$ is the damping parameter.

- If the input signal contains only low frequencies ($s \to 0$), then $\theta_p/\tau_p \approx 1/K$ and only K is accurately identified.
- If the input signal contains only high frequencies ($s \to \infty$), then $\theta_p/\tau_p \approx 1/I$ and only I is accurately identified.
- If the input signal has sufficient frequency content around the system natural frequency ($s \to \omega_n$), then $\theta_p/\tau_p \approx 1/(2K(1 + \xi))$ and B can be accurately identified if K and I are known.

In general, the input signal should have a frequency content of at least twice ω_n. The experiments [23], [35] performed on the human forearm with a sinusoidal force input have estimated that the natural frequency for the human elbow joint is as high as 25 Hz. Although the muscle afferents are known to respond to frequencies in excess of 100 Hz [26], the musculoskeletal system acts as a second-order, low-pass filter with a much lower corner frequency [32], [33]. We therefore felt that the airjet system should have a frequency content up to 100 Hz.

The force amplitude should be large enough to produce measurable deflection at the highest frequency. If the arm is initially at rest, then for a constant initial acceleration

the force is

$$F = \frac{I}{l^2}\left(\frac{2d}{t_r^2}\right) \tag{3}$$

where $d = 0.2$ mm is the smallest deflection reliably measured by the Optotrak ($SNR = 4$) and $t_r = 0.01$ s is the rise time (100 Hz). For a typical adult male, the distance from the elbow to wrist is 0.25 m, and the moment of inertia of the forearm and hand about the elbow is 0.06 Nms² [8]. The required perturbation force is then 4 N at 100 Hz. Higher forces and frequencies may be impractical. Because the force depends on the square of time or frequency, a higher frequency requires considerably more force. Excessively high forces may not be suitable for a small perturbation analysis to derive a linearized characterization of the true nonlinear arm dynamics. Projecting ahead the requirements for perturbation at the shoulder joint, the added inertia of the forearm plus upper arm is roughly canceled by the increased lever arm through which the force acts.

The airjet system described in this paper is a controllable bistable device which generates binary forces rather than graded responses. Hence an input type based on pseudorandom binary sequences (PRBS) is natural for this device. Theoretical advantages of identification methods based on PRBS inputs have been extensively detailed in the literature [10], [24], [25], and their use has been advocated for motor control research [13], [17].

III. AIRJET THEORY

The airjet (Fig. 1) is comprised of guide tubes, fluidic valve, and nozzle. In this section, an airjet theory developed from a two-dimensional analysis is discussed in four steps: 1) force versus mass flow rate, 2) guide tubes, 3) nozzle, and 4) fluidic valve.

A. Force Versus Mass Flow Rate

First, we determine the force generated in steady state given the inlet and exit pressures and areas. This can be done simply by momentum conservation, the ideal gas equation, and a continuity equation [21].

To simplify the problem, consider the airjet with fixed point support (Fig. 1). A control volume is constructed around the airjet and is closed at the inlet and two exits. The net force F acting on the airjet by its supporting structure must be equal to the time rate of change of momentum of the contents of the control volume. If the flow is steady, this balance may be expressed as

$$F = (\dot{m}_1 u_1 - \dot{m}_2 u_2)i + \dot{m}_i u_i j \tag{4}$$

where subscript i stands for the inlet port, subscripts 1 and 2 stand for the two exit ports, $\dot{m}_j$ is the mass flow rate and u_j is the flow velocity for port $j = \{i, 1, 2\}$, and i, j are the x, y unit vectors (Fig. 1). The mass flow rates can be further written as:
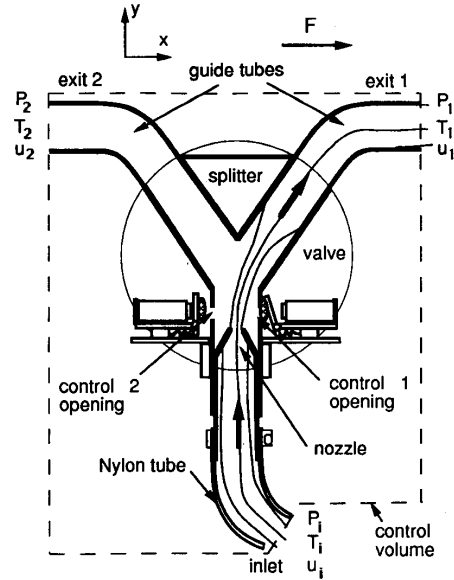
$$\dot{m}_j = \rho_j A_j u_j \tag{5}$$

Fig. 1. Schematic diagram of airjet system.

where A_j is the area and ρ_j is the local flow density of port $j = \{i, 1, 2\}$. In our design, $A_1 = A_2 \approx A_i$.

At the airjet exits, the static pressures P_1, P_2 and temperatures T_1, T_2 are assumed to equal atmospheric pressure P_0 and temperature T_0 where subscript 0 stands for ambient quantities. This is a reasonable assumption because the flow is fully expanded in the guide tubes. The high-pressure air comes to the nozzle inlet through a long flexible nylon tube whose heat conductivity is sufficiently high. It is reasonable to assume that the temperature at the nozzle inlet is close to ambient temperature ($T_1 = T_2 \approx T_i = T_0$). The inlet pressure P_i is much higher than the exit pressures ($P_i/P_0 \approx 4$-6). The ideal gas equation, as applied to the inlet and exits, is

$$P_j = \rho_j T_j R \tag{6}$$

where $j = \{i, 0, 1, 2\}$ and $R = 287$ m²/(s²°K) is the gas constant for air. For air at sea level conditions and $T_0 = 288°K$, $\rho_0 = 1.23$ kg/m³ and $P_0 = 101.3$ kPa. From above, $\rho_1 = \rho_2 = \rho_0 \ll \rho_i$. Neglecting the small quantity of the flow sucked in through the control openings on the fluidic valve, the continuity equation is

$$\dot{m}_i = \dot{m}_1 + \dot{m}_2. \tag{7}$$

In the steady state, either $\dot{m}_1$ or $\dot{m}_2$ is equal to zero, but not both. Assume $\dot{m}_1 \neq 0$ and $\dot{m}_2 = 0$; hence $\dot{m}_i = \dot{m}_1$. From (5),

$$u_i = \frac{\rho_1 A_1}{\rho_i A_i} u_1 \tag{8}$$

Since $\rho_i \gg \rho_1$ and $A_1 \approx A_i$, then $u_i \ll u_1$. Hence from (5),

$$F \approx \rho_1 A_1 u_1^2 i = \dot{m}_1 u_1 i. \tag{9}$$

B. Guide Tubes

The guide tubes turn the flow by 90°. Because the air-jet's force is proportional to the square of the exit flow velocity, the focal point in designing the guide tubes is to minimize any loss from shock waves and turbulence. Unfortunately, sensitivity to operating conditions constrain the design.

The static flow pressures, the temperatures, and the densities at both ends of the guide tubes are the same and equal to the atmospheric values. The air jet shoots into a guide tube inlet at sonic or supersonic speed. The requirement here is that the jet should not spill over at the inlet; that is to say, the jet should not be split into both guide tubes at the same time.

Theoretically, one may use a diffuser to reduce the jet flow to subsonic, turn the subsonic flow by the desired angle, and finally use a nozzle to accelerate the flow back to supersonic. In this ideal case, the loss is minimized because there is no shock wave formed. Yet this is impractical for two reasons [19]. One is the starting problem. Suppose that a fixed geometry, ideal shock-free diffuser is designed based on the steady jet flow Mach number M. When the jet flow is switched into the diffuser, a shock wave is formed in front of the diffuser. Even though the inlet jet flow reaches M, the shock wave does not go away because the flow behind the shock wave has a lower Mach number and the jet flow will spill over. The other problem is that boundary layer growth prevents diffusion to $M = 1$, because there is a minimum passage area at which the Mach number can be one. For a given Mach number of the jet flow, the Mach number at the point of minimum area (throat) would be very sensitive to the thickness of the boundary layer there [19], [21]. Perturbation in the boundary layer would result in a shock wave, which would be expelled to a position ahead of the diffuser entrance.

Given these difficulties, we simply use uniform dimension tubing with slightly large cross-section area. If the jet area is much smaller than the tubing area, the flow will not spill over at the guide tube inlet. Such a design also implies that the flow at the guide tube exit must be subsonic and the loss inside the tube is quite large.

C. Nozzle

The function of the nozzle is to convert the potential energy in pressurized gas into kinetic energy. Since it was argued in the previous section that supersonic flow does not help much in the gain of thrust, it is enough to design a convergent nozzle to convert high-pressure air into sonic flow. The problem now becomes to determine the nozzle exit area given the inlet pressure and the required mass flow rate. The design is based on two-dimensional channel flow theory [19]. Here we only list the main results. Assuming the nozzle is choked, the unit flow rate at the choke point is given by

$$\rho_{ne} u_{ne} = \gamma^{1/2} \left(\frac{2}{\gamma + 1} \right)^{\gamma + 1/2(\gamma - 1)} \frac{P_{it}}{(RT_{it})^{1/2}} \qquad (10)$$

where the subscript ne refers to the choke point or nozzle exit, the specific heat ratio $\gamma = 1.4$ for air, $T_{it} = T_0$ is the inlet total temperature, and P_{it} is the inlet total pressure. P_{it} can be found from (6) and (8):

$$P_{it} = P_i + \frac{1}{2} \rho_i u_i^2 = P_i + \frac{1}{2} \rho_0 \frac{P_0}{P_i} u_i^2. \qquad (11)$$

The nozzle throat area A_{ne} can be found from

$$\dot{m}_i = A_{ne}(\rho_{ne} u_{ne}). \qquad (12)$$

D. Fluidic Valve Geometry

The fluidic switching valve, the key component of the airjet system, is a bistable device that determines the airjet frequencies. Because it is a fluidic device, its normal operation is sensitive to geometry.

The fluidic valve operates by the Coanda effect. Consider an incompressible, turbulent, two-dimensional wall jet discharging into a quiescent fluid medium of large extent. Because of viscous interaction between the jet and the surrounding fluid, the jet entrains its surrounding medium. Essentially, the fluid in the medium is set into motion by the discharging jet. Under steady-state conditions, the motion of the jet and the entire surrounding medium becomes established in a particular flow pattern. If the boundary is positioned as shown in Fig. 2, the flow pattern on the side of the jet is significantly changed. The entrainment of fluid into the jet causes a depression between the jet and the boundary. The resulting pressure difference across the jet causes it to bend towards the wall and the depression is increased. This process is cumulative and finally the jet attaches to the wall as in Fig. 2. The pressure difference across the jet balances the force due to the radial acceleration v^2/r where v is the jet velocity and r is the radius of the jet, which in turn is close to the fluid flowing in a curved path. The pressure difference acting on faces $W_0 W_1$ and $W_0 W_3$ of the control volume $W_0 W_1 W_2 W_3$ causes fluid to be reversed into the jet in order to supply the entrained fluid. The situation is stable because a smaller radius of curvature could require a lower bubble pressure to balance the increased acceleration, but this would draw in more fluid than required for entrainment so the bubble would grow back to its original curvature. The converse is true if the radius of curvature increases from equilibrium.

A splitter divides the jet into two directions. In Fig. 1, control opening 1 is blocked and control opening 2 is open. The jet flow attaches to the right wall according to the Coanda effect, as the splitter and the right wall form a duct to guide the flow. If control opening 2 is closed and 1 is opened, the flow switches to the left. The switching must be stable at high frequencies and the flow should not spill over at the splitter.

An approximate model for the fluidic valve is given in Appendix A. In this Appendix, it is assumed that the basic dimensions of the valve are given, namely the nozzle width b_{ne} and the distance between the nozzle and attach-
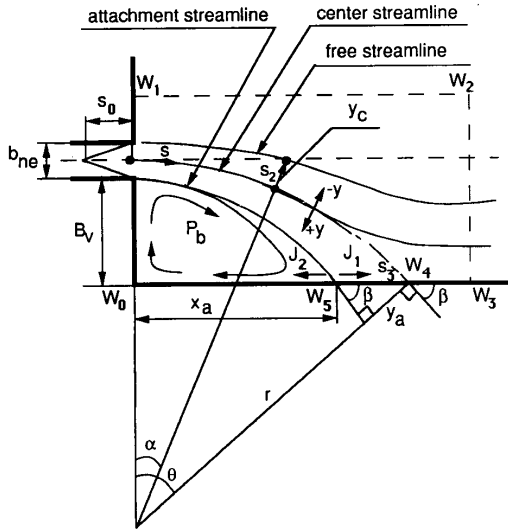
Fig. 2. Analytical model for jet attachment.

ment wall B_r. Expressions are found for the location of the attachment point a_3, the crossover point of the free streamline with respect to the nozzle axis, and the average pressure in the side bubble. Information from this Appendix is used in the next section to help set design parameters.

IV. AIRJET MECHANICAL DESIGN

To follow the two dimensional calculations above and in Appendix A, the cross section of the valve and the nozzle should be rectangular to prevent secondary flow (the flow in the plane perpendicular to the flow direction) induced by the pressure gradient across the jet. The inlet tubing of the nozzle and the guide tube are not necessarily restricted to be rectangular or square in shape; they can be circular or elliptical.

We constructed the switching valve and nozzle from square cross section brass tubing, which has high strength and can be made thin-walled to reduce weight. The switching valve contains three tubes of equal cross section, assembled by soldering. The splitter is formed from two tubes machined with the same angle at their ends. The control openings are made on the third piece. We constructed the guide tube from round cross section copper tubing, which can be bent easily; it was attached to the valve by soldering. Eventually, the whole assembly will be fabricated in plastic by using, for example, stereolithography apparatus.

The nozzle is made by pinching two sides of a tube in a precise mold. A standard connector can be soldered on the other end for the flexible tubing which goes to the air supply. The brass tube for the nozzle has a dimension one size down from the switching valve to allow sliding inside the valve for minor adjustments in the distance l_s to offset modeling errors.

A. Exit Dimensions

The first requirement is that the airjet should achieve a specified force level, namely 4 N. Based on (9), the force level can be raised by increasing the exit velocity, the exit area, or both. The exit velocity is limited by the speed of sound, as discussed in Section III-B. In practice, a further limit is imposed by spillover and a requirement that the jet cross section is much smaller than that of the guide tube. Hence, increasing the exit area is the main option.

To determine the maximum attainable exit velocity and the exit area required to achieve a 4 N force, we constructed a preliminary version of the airjet to perform experiments. The guide tubes had a diameter of 7 mm. The inlet pressure was increased until the jet spilled over, at about 220 kPa (40 psi), at which the force was measured as 2 N. The flow velocity at the guide tube exit was estimated by placing a plate attached to a force sensor in front of the exit. From the measured force and (9), we estimated $u_1 = 200$ m/s; this estimate is approximate, and a more accurate estimate would require special instrumentation.

The flow velocity is primarily determined by the geometry of the chamber and by the inlet pressure at which the jet spills over. Scaling the airjet dimensions is not expected to significantly change the flow velocity. From (9) with $F = 4$ N and $u_1 = 200$ m/s, the desired guide tube area can be estimated as $A_1 = 8 \times 10^{-5}$ m^2. From (5), the mass flow rate $\dot{m}_1 = 0.02$ kg/s. The valve exit up to the guide tube is made from square-section tubing. From the desired A_1, we find that $b_{ve} = h_{nz} = 9$ mm.

After the final version of the airjet was built, we rechecked the flow velocity, and according to expectations it was again 200 m/s.

B. Nozzle Dimensions

The nozzle throat area A_{ne} can be found from (10)–(12), but first P_i must be determined. As mentioned in Section III-A, it is desirable that $P_i/P_0 \approx 4$–6; we set this ratio at 5, or $P_i = 550$ kPa. From the value of u_1 above, we calculate from (11) that $P_{it} - P_i = 4.6$ kPa, and hence $P_{it} \approx P_i$.

The nozzle throat area can then be calculated as $A_{ne} = 1.5 \times 10^{-5}$ m^2. As mentioned in Section III-A, we also selected $A_i = A_1 = A_2$ and constructed the nozzle from square cross section tubing with $h_{nz} = 9$ mm. The nozzle width b_{ne} can then be found as $b_{ne} = A_{ne}/h_{nz} = 1.7$ mm.

C. Valve Dimensions

The remaining dimensions to be determined are the distance B_r between the nozzle and the wall, the splitter angle γ, the distance l_s between the nozzle exit and the splitter, and the control opening b_{rc} (Fig. 3). Dimensions B_r, γ, and l_s are related. From Figs. 1 and 2, it is seen that the free streamline must be bent passing through the line connecting the nozzle and the splitter to avoid spillover. B_r must be larger than the jet dimension at $s = l_s$, but should not be too large in order to have a high frequency
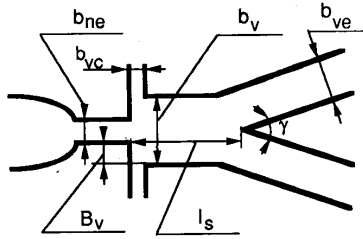
Fig. 3. Valve dimensions for the airjet.

response. The larger is l_s, the smaller can be γ. A smaller γ is desirable because a larger γ requires a larger acceleration to swing the jet, and the switching frequency would be lower. In the other words, increasing γ increases the memory and slows down the switching speed. We chose $\gamma = 20°$.

As mentioned at the beginning of this section, for reasons of simplicity of fabrication, the same square tubing was selected for the three parts of the switching valve. The value of B_r, is then predetermined at 3.6 mm since the square tubing side is 9 mm and the nozzle width is 1.7 mm.

To determine l_s, we use the analytical model in Appendix A to find the crossing point and the jet attachment point (here they are 5.7 and 9.1 mm). Using (14), for l_s increasing from 20 to 40 mm, it is found that the jet doubles its dimension. In general, the splitter should be three to six times the crossing point.

The control opening b_{rc} should be as large as possible, but is limited by the control device's force. The maximum force required to overcome the low-pressure bubble is theoretically given by (29). Experimentally, we found that a reasonable value is $b_{rc} = 3$ mm. The numerical values of the airjet parameters are summarized in Table I.

D. Force Sensor Design

A beam type of force sensor, with two platforms at its ends and two pairs of strain gages at each side forming a bridge, supports the airjet (Fig. 4). The key dimensions are the beam length l, width w, and thickness d; they are based on the dynamics of the sensor, the cuff, and the airjet.

The beam length l is mainly based on the cuff. If there is a rotation torque on the cuff along the forearm, it is very difficult to eliminate a radial rotational skin motion relative to the bone. In order to prevent this skin motion, the force has to intersect the axis of the forearm. To do so, we use a rigid bar to connect the cuff and the sensor (Fig. 5). The length therefore is determined by the wrist thickness (≈ 20 mm). The beam width w is not as crucial as its thickness because it has less influence on the bending moment inertia. In order to give the airjet good support and eliminate vibration in the nonforce directions, we set $w = 2l$. The platforms at the ends of the sensor are for mounting. Their thickness d_p should be at least twice the
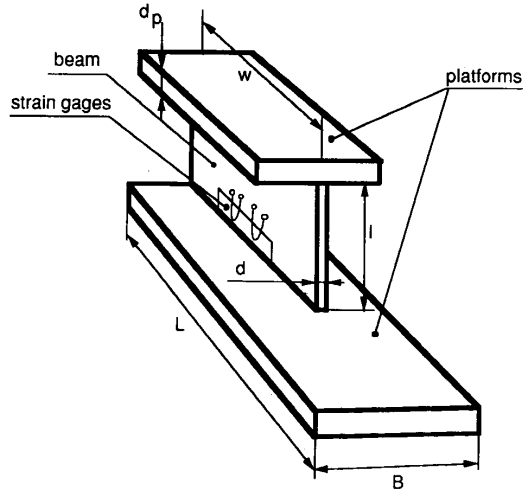

Fig. 4. Force sensor platform for the airjet.
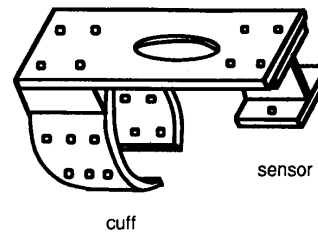
Fig. 5. Cuff design for attachment to wrist and mount for airjet.

TABLE II
SENSOR PARAMETERS

d	2.54 mm
l	12.7 mm
w	25.4 mm
d_p	4 mm
L	30 mm
B	30 mm

thickness of the beam d. The other dimensions are designed based on the fit of the airjet.

It would be desirable for the beam to be as thin as possible to yield a large strain, but the thinness is limited by the strain gage's maximum strain ϵ_{max} and the force transmissibility in the frequency range of interest. The maxi-
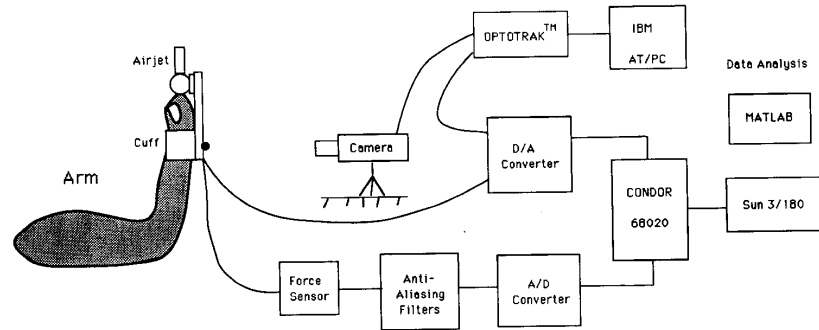
Fig. 6. Diagram of full airjet system.

mum strain in the beam from its dimension is given by [12]

$$\epsilon_{max} = \frac{Fld/2}{EI} \tag{13}$$

where F is the force, $E = 7.056 \times 10^{10}$ N/m^2 is the modulus of elasticity, and I is the area moment of inertia ($d^3w/12$). The material is 2024-T6/T351 aluminum. If we set the safety factor of 2 on the maximum strain, then the minimum thickness can be found from (13) as $d_g = 1.1$ mm.

Force transmissibility requires that the beam is sufficiently stiff so that the natural frequencies are significantly larger (at least two to three times) than the frequency range of the system under study, and hence imposes a limit on the minimum thickness. A dynamic model for the force sensor is derived in Appendix B, and an expression for the natural frequencies appears as (40). If we set $\omega = 200$ Hz as the lowest acceptable beam frequency, we find that the minimum thickness due to force transmissibility is $d_f = 2.5$ mm.

Finally, the beam thickness is given by $d = \max \{d_g, d_f\} = 2.5$ mm. Thus, force transmissibility imposes a more stringent limit than does maximum strain. The sensor parameters are summarized in Table II. The force sensor was calibrated with a commercial six-axis force sensor (Barry Wright Controls FS6-120A). We tested the frequency response of the force sensor by imparting a force impulse with a sharp tap. It was found that $\omega = 170$ Hz, close to the theoretical value.

E. Cuff Design

The airjet is attached to the wrist with a special cuff (Fig. 5). A subject's wrist is first immobilized with an individually fitted plastic cast made from Aquaplast™; this cast extends from the hand halfway towards the elbow. Over the plastic cast, a cylindrical aluminum clamp of elliptical cross section is fastened by means of 12 pressure screws, which provide good mechanical attachment without affecting blood circulation.

Attached to the clamp is an aluminum lever arm which runs distally in front of the hand. The airjet is attached to the distal end on the side of the hand through the force sensor. The reason for this arrangement is twofold: 1) when the airjet is aligned with the long axis of the forearm, no torque on the wrist cuff is induced; and 2) the torque on the elbow due to the airjet is increased with the longer lever arm.

V. PERFORMANCE ASSESSMENT

A. Control System

By simultaneously and rapidly blocking and unblocking the control openings in the valve walls of the airjet (Figure 1), the jet can be made to flip from one wall to the other. The control action required is merely to cover or uncover an opening, and this has been accomplished with two small solenoids and sprung flappers. Because the flappers are light and small, they can be lifted rapidly by the solenoids to achieve high frequency bandwidth. The lifting action loads the springs, which return the flapper to block an opening when the solenoid is deactivated; a piano felt covering on the flapper surface prevents bouncing.

A diagram of the complete system is given in Fig. 6. The control system runs on the CONDOR real-time control architecture [30], comprised of a Sun 3/180 computer and an associated Motorola 68020 microprocessor system on a VME bus. For force sensing, the analog signals from the strain gages are passed through a 2B31J signal conditioner (Analog Devices), which has an instrumental amplifier, a buffer amplifier, and a three-pole Bessel filter for antialiasing with cutoff frequency 200 Hz. The conditioned force signal is sampled at 2000 Hz through an ADC. The Optotrak™, which is interfaced to an IBM PC/AT, is synchronized with the CONDOR system through the DAC.

B. Airjet and Force Sensor

The airjet system has been extensively tested, and meets almost all of the initial specifications. In the test, the airjet system is secured on a rigid table. The air supply is from a 14 000 kPa nitrogen tank regulated down to 550 kPa.

Fig. 7 is the step response, whose main features are listed in Table III. A rise time less than 1 ms shows that the jet stream switching is fast. There is a 5 ms delay to the command issued from the computer, which does not
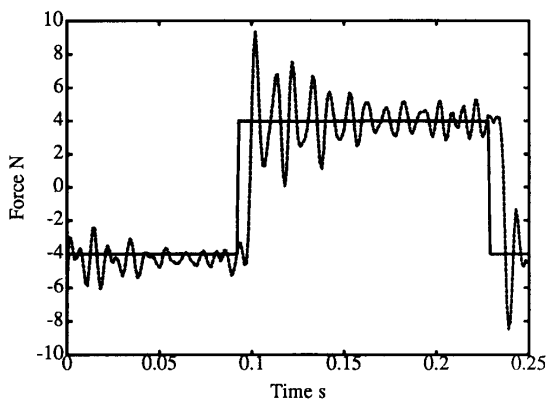
Fig. 7. Step response: desired force (solid line) versus measured force (dotted line).
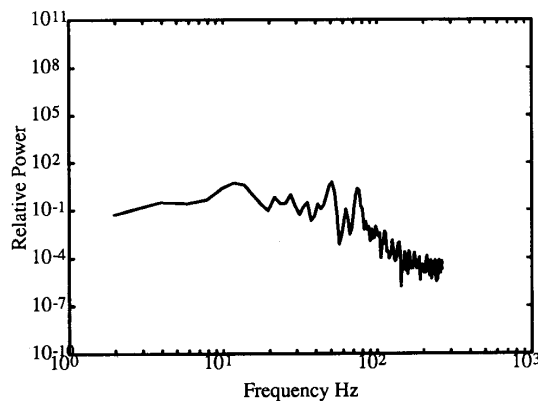

Fig. 8. Normalized power spectrum of random perturbation.

TABLE III
FORCE STEP RESPONSE

Steady-state force	4 N
Overshoot	100%
Damping ratio	0.06
Settling time	100 ms
Rise time	1 ms
Delay to input	5 ms

cause a problem for system identification. The coil is apparently responsible for this delay, which limits the upper frequency. The sensor damping ratio is quite low.

The power spectrum of the random binary force perturbation is flat to 75 Hz (Fig. 8), and the usable frequency range extends to 150 Hz. Hence the airjet system frequency response exceeds the specifications. Above 75 Hz, the flow tends to go through one side of the airjet more than the other. Since the step response has shown that the fluid switching is less than 1 ms, the main problem must be due to the coil flapper device, which operates below 100 Hz. Because of the suction force at the control openings on the airjet, the switching frequency of the coil flapper device is further reduced.

The speed of the electromagnetic device can be increased with special step inputs. A large but brief initial current pulse followed by a sustained but much smaller maintenance current step would rapidly lift and hold the flapper and expose the control opening to ambient pressure. The coil temperature would not rise excessively since it is proportional to the time integral of the pulse plus step. Moreover, the current required to hold a flapper closed is small because of the suction.

The acoustic noise produced by the airjet was measured with a precision sound level meter (type 2203 from Brüel and Kjaer). The noise level at 15 cm was 80 dB between 22 and 1000 Hz and increased to 110 dB above 1 kHz. When participating in experiments, subjects wear ear protectors which lower the peak noise to 80 dB. Subjects report that they do not feel uncomfortable with the noise level.

C. Cuff

We examined how well the cuff mechanically couples the airjet to the arm by measuring the cuff's motion. In the test, the subject's elbow, wrist, and hand are fixed to a rigid support. The response of cuff motion to a step in airjet force was measured in two cuff locations: at the wrist and at the tip of the lever arm.

At the wrist, the cuff movement was between 0.1 and 0.2 mm, which is the same as the lowest detectable wrist movement specified in Section II. This shows that the

noise in the wrist movement data due to the compliance of the tissue at the wrist is small. At the tip, the cuff motion was 0.4 mm, twice as large as the motion at the wrist. To ascertain whether this motion influences the force transmission from the airjet to the arm, let us assume that the compliance of tissue and the bonds is approximately linear for small deformations; of course, for large deformations the tissue mechanics are nonlinear. In Fig. 9(a), we plot the frequency response of the transfer function, the ratio of the angular movement of the lever arm about the wrist with forearm fixed, and of the force. The frequency response is flat at least to 300 Hz because the data are filtered with cutoff frequency at 200 Hz for antialiasing. Hence the force transmission is good. The validity of the linear model is demonstrated by the coherence function in Fig. 9(b).

VI. SUMMARY

A lightweight airjet system has been described for applying high-frequency stochastic perturbations to the unencumbered arm. A systematic design method has been presented based on a two-dimensional analysis. Design specifications, such as perturbation type, frequency content, and force magnitude have been set forth based on the properties of the human motor system and the position measurement system. Three components of the airjet—guide tube, nozzle, and fluidic switching valve—have been designed analytically using gas dynamics. A beam type of force sensor for measuring the airjet force has been designed. The force transmissibility is identified. Cuff design and data acquisition have also been discussed.

Test results for the airjet have been presented. Under normal operating conditions, the airjet system has a flat frequency response of 4 N to 75 Hz. The force transmis-
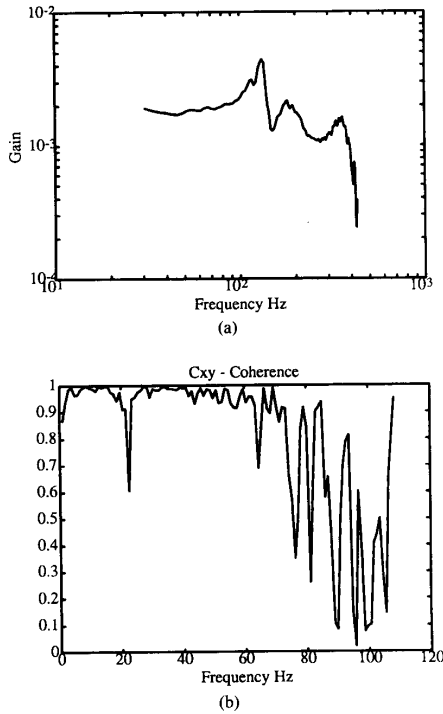
Fig. 9. (a) Frequency response of the cuff rotation. (b) Coherence function for cuff rotation.

sibility of the cuff to the wrist is assessed both in the time domain and in the frequency domain. The skin movement is insignificant with our cuff design. Using the airjet system, preliminary studies have been conducted on the elbow joint dynamics during posture and movement [3], [34].

Appendix A

Using a simplified wall attachment model [31], we will find the attachment point distance and the streamlines, which are important in designing the airjet system. The following assumptions are made.

1) The flow is steady, incompressible, and two-dimensional.

2) There is no interaction between the fluid and solid boundaries.

3) The jet velocity is uniform at the nozzle exit.

4) The nozzle width is small compared with the radius of curvature of the jet and the length of the attachment wall.

5) The pressure in the separation bubble is uniform up to the center line, and the center streamline is at ambient pressure.

6) The radius of curvature of the center line of the attached jet is in steady state.

7) The jet flow is independent of the separation bubble pressure.

8) In the bubble the flow entrained by the jet is equal to the returned flow.

9) The control flow is insignificant. The jet is pushed to the wall by the pressure gradient across the jet.

Velocity Profile of a Turbulent-Free Jet

This profile u for an infinitesimal aperture is given by Görtler's equation [20]:

$$u = U_{\max} \mathrm{sech}^2 \eta \tag{14}$$

where

$U_{\max}$ = maximum velocity of jet profile,
$\eta = \sigma y / s_1$, a nondimensional jet profile coordinate,
$\sigma = 12$, the jet spread factor which is an empirical constant,
y = distance perpendicular to the jet centerline, and
s_1 = distance from the aperture along the jet center line.

The jet momentum flux J per unit length is given by

$$J = \rho \int_{-\infty}^{\infty} u^2 \, dy = \frac{4}{3} \rho U_{\max}^2 \frac{s_1}{\sigma}. \tag{15}$$

The volume flow Q per unit length is given by

$$Q = \int_{-\infty}^{\infty} u \, dy = 2 U_{\max} \frac{s_1}{\sigma} = \sqrt{\frac{3 J s_1}{\sigma \rho}} \tag{16}$$

where $U_{\max} = \sqrt{3 \sigma J / 4 \rho s_1}$.

Because the nozzle exit is not an infinitesimal aperture, we need to place the origin of the flow a distance s_0 upstream of the nozzle where s_0 is chosen such that the volume flow Q out of the nozzle, as given by (16) above with $s_1 = s_0$, is the same as the volume flow Q_s of a jet with a uniform profile:

$$Q_s = u_{\mathrm{nc}} b_{\mathrm{nc}} = \sqrt{\frac{J b_{\mathrm{nc}}}{\rho}} \tag{17}$$

where b_{nc} is the nozzle width, u_{nc} is the nozzle exit velocity, and $J = \rho u_{\mathrm{nc}}^2 b_{\mathrm{nc}}$ for the uniform jet. Let $s_1 = s + s_0$ where s_0 is to be determined. Equating (16) and (17) at $s_1 = s_0$,

$$s_0 = \sigma b_{\mathrm{nc}} / 3. \tag{18}$$

Streamlines

The center streamline, the attachment streamline, and the free streamline (the jet free boundary) are shown in Fig. 2. The attachment streamline divides the flow: one portion returns to the bubble and the other proceeds downstream. The center streamline is assumed circular with unknown radius r. Let Q_y be the volume flow contained between the center streamline and y. Since the volume flow cannot cross a streamline, the equation of a streamline is

$$Q_y = \int_0^y u \, dy = U_{\max} \tanh \eta \tag{19}$$

where (14) was substituted. Let $Q_{y_a} = Q_s / 2$ be the volume flow between the center line and the attachment streamline, located at $y = y_a$. From (17) and (19),

$$\tanh \eta_a = \sqrt{s_0 / s_1} \tag{20}$$

where $\eta_a = \sigma y_a / s_1$. At the free streamline, $y = -y_f$, and similarly

$$\tanh \eta_f = \tanh \eta_a \tag{21}$$

where $\eta_f = \sigma y_f / s_1$.

The streamline calculation, which is based on the assumed centerline, is valid only before the attachment point. After the attachment point, the centerline assumption and the jet velocity profile (14) are not valid, but this region is unimportant here.

Momentum-Flux Equation

Assume that the momentum flux is conserved in a volume surrounding the attachment point W_4, and that the angle of the input momentum flux J is the same as the angle β made by the extended centerline [6]. Let J_1 be the momentum flux in the direction along the wall and J_2 the momentum flux returned to the bubble:

$$J_1 = \rho \int_{-\infty}^{y_a} u_{s_3}^2 \, dy, \qquad J_2 = \rho \int_{y_a}^{\infty} u_{s_3}^2 \, dy$$

where s_3 is the centerline distance from the aperture to the attachment point W_4, and u_{s_3} is the velocity profile across the jet there. Then

$$J \cos \theta = J_1 - J_2. \tag{22}$$

Substituting (19) and rearranging

$$\cos \theta = \tfrac{3}{2} \tanh \eta_{s_3} - \tfrac{1}{2} \tanh^3 \eta_{s_3} \tag{23}$$

where $\eta_{s_3} = \sigma y_a / (s_0 + s_3)$.

Geometric Relationships:

The six variables to be determined are s_0, s_3, r, θ, y_a, and $x_a = \overline{W_0 W_5}$. In addition to the three equations (18), (19) with s replaced by s_3, and (23), the necessary other three equations are derived geometrically (Fig. 2):

$$r\theta = s_3 \tag{24}$$

$$r \sin \theta = x_a + y_a / \sin \theta \tag{25}$$

$$r(1 - \cos \theta) = B_r + b_{\text{nc}} / 2. \tag{26}$$

Free Streamline Crossing Point

In the design it is necessary to know where the free streamline crosses the nozzle axis. This point W_f corresponds to $s = s_2$, and is found from (21) and the following additional relations:

$$r = (r + y_c) \cos \alpha \tag{27}$$

$$s_c = r\alpha \tag{28}$$

Pressure Inside Bubble

To find this pressure P_b, first consider the control volume formed by the centerline and the walls. The pressure forces acting on the control volume are the ambient pressure P_0 and the bubble pressure P_b; their sum equals the change of momentum. Since P_b and P_0 act on the unit depth surface $r - r \cos \theta$, the net pressure force is $r(1 - \cos \theta)(P_b - P_0)$. The change in momentum is $(J_1 - J_2) - J$, so that the momentum equation is

$$r(1 - \cos \theta)(P_b - P_0) = (J_1 - J_2) - J.$$

If $\theta = 90°$, then $J_1 = J_2$, and

$$P_b = P_0 - J/r \tag{29}$$

APPENDIX B

The force sensor can be modeled as a Bernoulli–Euler beam. One end ($x = 0$) is clamped and the other end ($x = l$) experiences a vertical force F from the airjet. The equilibrium equation is [12]

$$(EIw'')'' = 0 \tag{30}$$

where $w(x)$ is the vertical displacement at point x for a horizontal beam. The solution to (30) is the cubic polynomial

$$w(x) = a_1 \left(\frac{x}{l}\right)^2 + a_2 \left(\frac{x}{l}\right)^3 \tag{31}$$

where $w(0) = w'(0) = 0$. We identify as generalized coordinates the endpoint dislacement $v_1 = w(l) = a_1 + a_2$ and slope $v_2 = w'(l) = (2a_1 + 3a_2)/l$. In terms of the generalized coordinates, (31) becomes

$$w(x) = \phi_1(x) v_1 + \phi_2(x) v_2 \tag{32}$$

where $\phi_1(x)$ and $\phi_2(x)$ are the shape functions

$$\phi_1(x) = 3\left(\frac{x}{l}\right)^2 - 2\left(\frac{x}{l}\right)^3$$

$$\phi_2(x) = -l\left(\frac{x}{l}\right)^2 + l\left(\frac{x}{l}\right)^3.$$

Lagrange's equation is

$$\frac{d}{dt}\left(\frac{\partial T}{\partial \dot{v}_i}\right) - \frac{\partial T}{\partial v_i} + \frac{\partial V}{\partial v_i} = q_i \qquad i = 1, 2 \tag{33}$$

where $q_1 = F$, $q_2 = 0$, and

$$V = \tfrac{1}{2} \int_0^l EI(w'')^2 \, dx \tag{34}$$

$$T = \tfrac{1}{2} \int_0^l \rho A(\dot{w}^2) \, dx + \tfrac{1}{2} M \dot{v}_1^2. \tag{35}$$

For the kinetic energy, we model the airjet as a mass $M = 0.175$ kg at the end of the beam. Also, $\rho = 2.7 \times 10^3$ kg/m^3 and $A = dw$. Substituting (34) and (35) into (33), we obtain a matrix equation:

$$M\ddot{v} + Kv = q \tag{36}$$

where $v = (v_1, v_2)$, $q = (F, 0)$, and

$$m_{ij} = \int_0^l \rho A \phi_i(x) \phi_j(x)\, dx + M\phi_i(l)\phi_j(l)$$

$$k_{ij} = \int_0^l EI\phi_i''(x)\phi_j''(x)\, dx.$$

Solving

$$M = \frac{\rho A l}{420}\begin{bmatrix} 420M/(\rho A l) + 156 & -22l \\ -22l & 4l^2 \end{bmatrix} \quad (37)$$

$$K = \frac{EI}{l^3}\begin{bmatrix} 12 & -6l \\ -6l & 4l^2 \end{bmatrix}. \quad (38)$$

The natural frequencies (36) are obtained by solving the characteristic equation

$$|K - \omega^2 M| = 0. \quad (39)$$

The solutions are

$$\omega^2 = \frac{EI(2520M \pm 24\sqrt{3}\sqrt{208\rho^2 A^2 l^2 + 1680\rho A l M + 3675M^2}) + 612\rho A l EI}{\rho^2 A^2 l^5 + 12\rho A l^4 M}.$$

REFERENCES

[1] C. H. An, C. G. Atkeson, and J. M. Hollerbach, *Model-Based Control of a Robot Manipulator*. Cambridge, MA: MIT, 1988.
[2] Analog Devices, *1984 DataBook: Modules and Subsystems*. Analog Devices, Inc., 2 Tech. Way, P.O. Box 280, Norwood, MA 02062, 1984.
[3] D. J. Bennett, Y. Xu, J. M. Hollerbach, and I. W. Hunter, "Mechanical properties of the human arm during voluntary movement," in *Proc. Can. Med. Biol. Eng. Conf.*, Winnipeg, June 10-12, 1990 pp. 89-90.
[4] C. Billian and G. I. Zahalak, "A programmable limb testing system and some measurements of intrinsic muscular and reflex-mediated stiffnesses," *J. Biomech. Eng.*, vol. 105, pp. 6-11, 1983.
[5] E. Bizzi, W. Chapple, and N. Hogan, "Mechanical properties of muscles: Implications for motor control," *Trends Neurosci.*, vol. 5, no. 11, pp. 395-398, 1982.
[6] C. Bourque and B. G. Newman, "Reattachment of a two dimensional incompressible jet to an adjacent flat plate," *Aeronaut. Quart.*, vol. XI, p. 201ff, 1960.
[7] S. C. Cannon and G. I. Zahalak, "The mechanical behavior of active human skeletal muscle in small oscillations," *J. Biomechan.*, vol. 15, pp. 111-121, 1982.
[8] J. E. Colgate, "The design of a dynamics measuring device," Dep. Mechan. Eng., M.S. Thesis, MIT, Jan. 1986.
[9] J. R. Dufresne, V. S. Gurfinkel, J. F. Soechting, and C. A. Terzuolo, "Response to transient disturbances during intentional forearm flexion in man," *Brain Res.*, vol. 150, pp. 103-115, 1978.
[10] P. Eykhoff, *System Identification: Parameter and State Estimation*. New York: Wiley, 1974.
[11] A. G. Feldman, "Functional tuning of the nervous system with control of movement or maintenance of a steady posture III. Mechanographic analysis of the execution by man of the simplest motor tasks," *Biophys.*, vol. 11, pp. 766-775, 1966.
[12] Y. C. Fung, *Foundations of Solid Mechanics*. Englewood Cliffs, NJ: Prentice-Hall, 1965.
[13] I. W. Hunter and R. E. Kearney, "Dynamics of human ankle stiffness: Variation with mean ankle torque," *J. Biomechan.*, vol. 15, pp. 747-752, 1982.
[14] —, "Generation of random sequences with jointly specified probability density and autocorrelation functions," *Biol. Cybern.*, vol. 47, pp. 141-146, 1983.
[15] —, "Quasi-linear, time-varying, and nonlinear approaches to the identification of muscle and joint mechanics," in *Advanced Methods of Physiological Modeling*, 1987, pp. 128-147.
[16] L. Jones and I. W. Hunter, "Dynamics of human elbow joint stiffness," in *Proc. Canadian Med. Biol. Eng. Conf.*, Winnipeg, June 9-12, 1990, pp. 175-176.
[17] R. E. Kearney and I. W. Hunter, "System identification of human joint dynamics," *CRC Crit. Rev. Biomed. Eng.*, vol. 18, pp. 55-87, 1990.
[18] R. E. Kearney, I. W. Hunter, P. L. Weiss, and K. Spring, "Tilt-table/ankle-actuator system for the study of vestibulospinal reflexes," *Med. Biol. Eng. Comput.*, vol. 21, pp. 301-305, 1983.
[19] J. L. Kerrebrock, *Aircraft Engines and Gas Turbines*. Cambridge, MA: MIT, 1977.
[20] J. M. Kirshner and S. Katz, *Design Theory of Fluidic Components*. New York: Academic, 1975.
[21] A. M. Kuethe and C. Y. Chow, *Foundation of Aerodynamics: Bases of Aerodynamic Design*. New York: Wiley, 1976.
[22] F. Lacquaniti and J. F. Soechting, "Behavior of the stretch reflex in a multi-jointed limb," *Brain Res.*, vol. 311, pp. 161-166, 1984.
[23] J. M. Lanman, "Movement and the mechanical properties of the intact human elbow joint," Ph.D. Thesis, Dep. Psychol., MIT, 1980.
[24] L. Ljung, *System Identification: Theory for the User*. Englewood Cliffs, NJ: Prentice-Hall, 1987.
[25] P. Z. Marmarelis and V. Z. Marmarelis, *Analysis of Physiological Systems*. London: Plenum, 1978.
[26] P. B. C. Matthews, *Mammalian Muscle Receptors and Their Central Actions*. London: Edward Arnold, 1972.
[27] T. A. McMahon, *Muscles, Reflexes, and Locomotion*. Princeton, NJ: Princeton Univ., 1984.
[28] W. R. Murray, "Essential factors in modeling the modulation of impedance about the human elbow," Ph.D. Thesis, Dep. Mechanical Eng., MIT, 1988.
[29] F. A. Mussa-Ivaldi, N. Hogan, and E. Bizzi, "Neural, mechanical, and geometric factors subserving arm posture in humans," *J. Neurosci.*, vol. 5, pp. 2732-2743, 1985.
[30] S. Narasimhan, D. M. Siegel, and J. M. Hollerbach, "Condor: An architecture for controlling the Utah-MIT Dextrous Hand," *IEEE Trans. Robot. Automat.*, vol. 5, pp. 616-627, 1989.
[31] N. C. Sher, "Jet attachment and switching in bistable fluid amplifiers," ASME paper, 64-FE-19, Mar. 1964.
[32] J. F. Soechting and W. J. Roberts, "Transfer characteristics between EMG activity and muscle tension under isometric conditions in man," *J. Physiol. (Paris)*, vol. 70, pp. 779-793, 1975.
[33] R. B. Stein, "Peripheral control of movement," *Physiol. Rev.*, vol. 54, pp. 215-243, 1974.
[34] Y. Xu, I. W. Hunter, J. M. Hollerbach, and D. J. Bennett, "An airjet perturbation device and its use in elbow posture mechanics," in *Proc. 12th IEEE Int. Conf. Eng. Med. Biol.*, Philadephia, PA, Nov. 1-4, 1990, pp. 2116-2117.
[35] V. A. Yosef and G. F. Inbar, "Parameter estimation of the mechanical impedance of the forearm of the human-operator using Gaussian torque input," Dep. Elect. Eng., Technion-Israel Instit. Technol., Haifa, Israel, 1988.
[36] G. I. Zahalak and S. J. Heyman, "A quantitative evaluation of the frequency-response characteristics of active human skeletal muscle in vivo," *J. Biomechan. Eng.*, vol. 101, pp. 28-37, 1979.

Yangming Xu (S'89) received the B.S. degree from Northwestern Polytechnical University, China, in 1982, and the S.M. and Ph.D. degrees in aeronautics and astronautics from the Massachusetts Institute of Technology, Cambridge, in 1986 and 1991, respectively.

He is currently a Postdoctoral Fellow in the Department of Biomedical Engineering, McGill University, Montreal, P.Q., Canada. His research interests include system identification and control in biological robotic systems.

Ian W. Hunter (S'78-M'79) received the B.S. degree in science in 1974, the M.S. degree in 1975, and the Ph.D. degree in physiology in 1980, all from the University of Auckland, Auckland, New Zealand.

He is currently an Associate Professor of Biomedical Engineering at McGill University, Montreal, P.Q., Canada, and the General Motors Fellow of the Canadian Institute for Advanced Research. His interests include muscle mechanics, microrobotics, novel sensors and actuators, signal and system analysis (in particular, nonlinear system identification), optics, and architectures for high performance computation and control.

Dr. Hunter received the 1990 Canadian Biomedical Engineer of the Year Award.

John M. Hollerbach (M'85) received the B.S. degree in chemistry and the M.S. degree in mathematics from the University of Michigan, Ann Arbor, in 1968 and 1969, respectively, and the S.M. and Ph.D. degrees in computer science from the Massachusetts Institute of Technology, Cambridge, in 1975 and 1978, respectively.

He is the Natural Sciences and Engineering/Canadian Institute for Advanced Research Professor of Robotics at McGill University, jointly in the Departments of Mechanical Engineering and Biomedical Engineering. He has published several books and many papers in the area of robotics and biological motor control. He was Co-Chairman of the 1985 Engineering Foundation Conference on Biomechanics and Neural Control of Movement, and the Program Chairman of the 1989 IEEE International Conference on Robotics and Automation. He is a Technical Editor of the IEEE TRANSACTIONS ON ROBOTICS AND AUTOMATION, and a member of the Administrative Committee of the IEEE Robotics and Automation Society.

Dr. Hollerbach received an NSF Presidential Young Investigator Award.

David J. Bennett ('89) received the B.Eng. degree in electrical engineering from McGill University, Montreal, P.Q., Canada, in 1984 and the Ph.D. degree in brain and cognitive sciences from the Massachusetts Institute of Technology, Cambridge, in 1990.

He is currently a Postdoctoral Associate at the Department of Brain and Cognitive Sciences, Massachusetts Institute of Technology. His interests include system identification, motor control, and robotics.